THE ROYAL SOCIETY

*Received* 6 March 2002
*Accepted* 11 February 2003
*Published online* 2 May 2003

# Scaling properties and symmetrical patterns in the epidemiology of rotavirus infection

**Marco V. José[1*] and Ruth F. Bishop[2]**

[1]*Instituto de Investigaciones Biomédicas, Universidad Nacional Autónoma de México, Apartado Postal 70228, Ciudad Universitaria, CP 04510 México D.F. Mexico*
[2]*Department of Gastroenterology, Royal Children's Hospital, Flemington Road, Parkville Victoria 3052, Melbourne, Victoria, Australia*

The rich epidemiological database of the incidence of rotavirus, as a cause of severe diarrhoea in young children, coupled with knowledge of the natural history of the infection, can make this virus a paradigm for studies of epidemic dynamics. The cyclic recurrence of childhood rotavirus epidemics in unvaccinated populations provides one of the best documented phenomena in population dynamics.

This paper makes use of epidemiological data on rotavirus infection in young children admitted to hospital in Melbourne, Australia from 1977 to 2000. Several mathematical methods were used to characterize the overall dynamics of rotavirus infections as a whole and individually as serotypes G1, G2, G3, G4 and G9. These mathematical methods are as follows: seasonal autoregressive integrated moving-average (SARIMA) models, power spectral density (PSD), higher-order spectral analysis (HOSA) (bispectrum estimation and quadratic phase coupling (QPC)), detrended fluctuation analysis (DFA), wavelet analysis (WA) and a surrogate data analysis technique. Each of these techniques revealed different dynamic aspects of rotavirus epidemiology. In particular, we confirm the existence of an annual, biannual and a quinquennial period but additionally we found other embedded cycles (e.g. *ca*. 3 years). There seems to be an overall unique geometric and dynamic structure of the data despite the apparent changes in the dynamics of the last years. The inherent dynamics seems to be conserved regardless of the emergence of new serotypes, the re-emergence of old serotypes or the transient disappearance of a particular serotype. More importantly, the dynamics of all serotypes is multiple synchronized so that they behave as a single entity at the epidemic level.

Overall, the whole dynamics follow a scale-free power-law fractal scaling behaviour. We found that there are three different scaling regions in the time-series, suggesting that processes influencing the epidemic dynamics of rotavirus over less than 12 months differ from those that operate between 1 and *ca*. 3 years, as well as those between 3 and *ca*. 5 years. To discard the possibility that the observed patterns could be due to artefacts, we applied a surrogate data analysis technique which enabled us to discern if only random components or linear features of the incidence of rotavirus contribute to its dynamics. The global dynamics of the epidemic is portrayed by wavelet-based incidence analysis. The resulting wavelet transform of the incidence of rotavirus crisply reveals a repeating pattern over time that looks similar on many scales (a property called self-similarity). Both the self-similar behaviour and the absence of a single characteristic scale of the power-law fractal-like scaling of the incidence of rotavirus infection imply that there is not a universal inherently more virulent serotype to which severe gastroenteritis can uniquely be ascribed.

**Keywords:** rotavirus epidemic dynamics; detrending fluctuation analysis; higher-order statistics; spectral analysis; wavelet analysis

## 1. INTRODUCTION

Rotaviruses, members of the family Reoviridae, are the major aetiological agents of gastroenteritis in young animals and young children worldwide (Bishop 1986; Kapikian & Chanock 1996). Several studies have shown similar incidences of human rotavirus (HRV)-associated diarrhoea in industrialized and developing countries, suggesting that the control of this illness may not result from improvements in water supply, sanitation or hygiene, but may require an effective vaccine (De Zoyza & Feachem 1985).

Great variations in the distributions of serotypes occur over time and from place to place. Among the group A rotaviruses causing severe disease in young children, serotype G1 of VP7 has been associated most frequently with human disease (Estes & Cohen 1989; Padilla-Noriega *et al.* 1990; Bishop *et al.* 1991; Woods *et al.* 1992; Velazquez *et al.* 1993). Serotype G1 is the most common global serotype in circulation. Epidemics of serotypes G2, G3 and G4 have been detected from time to time in many different countries. Any proposed vaccine must provide good protection against the four epidemiologically significant HRV serotypes G1, G2, G3 and G4. In addition, new serotypes (G5, G6, G8 and G9) have also been identified.

*Author for correspondence (jose@servidor.unam.mx).

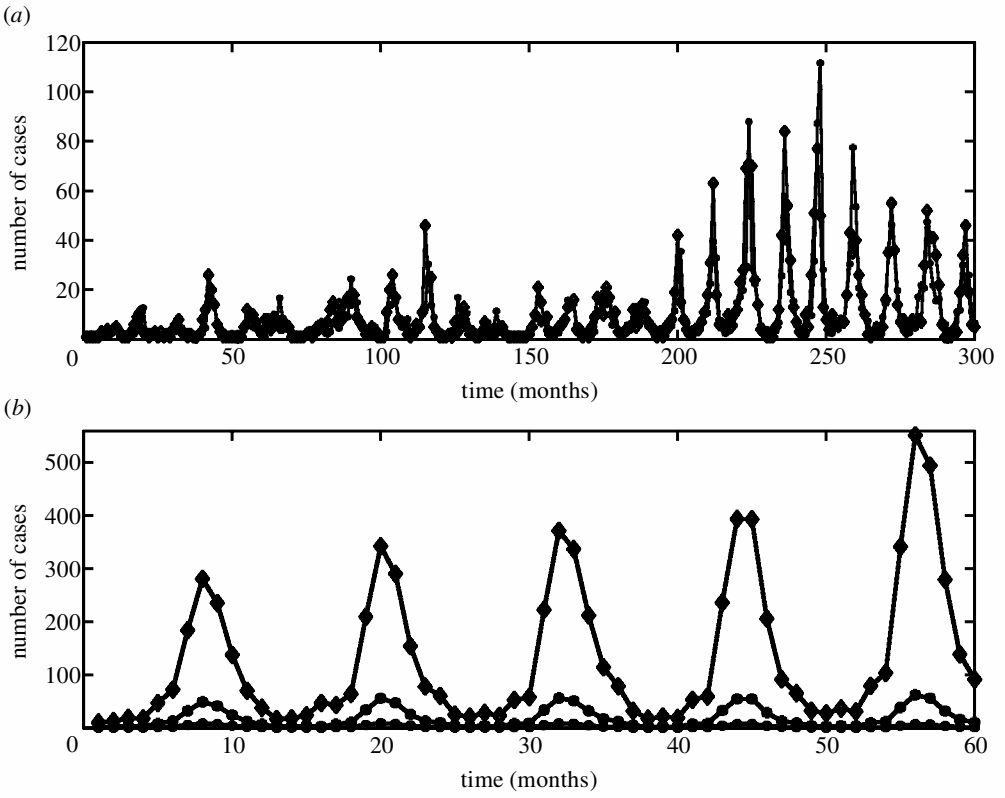


Figure 1. (*a*) Fitting of the monthly incidence of rotavirus in Melbourne, Australia from 1977 to 2000 based upon a SARIMA $(1, 0, 0) \times (3, 1, 0)_{12}$ model. Diamonds, actual data; asterisks, SARIMA model. (*b*) Monthly incidence forecasts of the rotavirus epidemic. Asterisks, expected incidence; diamonds, upper confidence interval of 95% of confidence; circles, lower confidence interval of 95% of confidence.

However, new serotypes have been reported to exist in several countries. For example in Australia, serotype G9 rotaviruses were first identified in 1997 (Masendycz *et al.* 2001) and have persisted since then. The finding of the re-emergence of certain serotypes (like G4 viruses) and the appearance of new serotypes provide opportunities for determining the dynamics of rotavirus epidemics, which could prove relevant for vaccine development strategies.

One of the most salient epidemiological features of human rotavirus gastroenteritis is its seasonality (Brandt *et al.* 1983; LeBaron *et al.* 1990; Ansari *et al.* 1991). Periodograms have been used for exploring seasonal and longer-term cycles (interepidemic periods) of rotavirus infection for serotypes G1, G2, G3 and G4 using hospitalization longitudinal data of the monthly incidence of rotavirus infection from the city of Melbourne, Australia during 1977–1993 (José *et al.* 1996). A clear evidence of a biennial peak in the epidemiology of rotavirus infection was detected. It was also noticed that there was probable existence of an interepidemic cycle of *ca.* 4.6–5.2 years' duration. The finding of this interepidemic cycle did not arise from the alternating incidence of the four serotypes because this peak appeared in the periodogram of each serotype (José *et al.* 1996).

Since 1994 to date, an apparent change in the pattern of incidence of rotavirus infection in Melbourne, Australia has been noted (see figure 1*a*). In this work we explore the overall dynamics of rotavirus infection. We used the longitudinal hospitalization data available of the monthly incidence of rotavirus infection (including all serotypes) from the city of Melbourne, Australia during 1977–2000. It was hypothesized that the recent appearance of a new serotype (G9) after 1977 or the re-emergence of certain serotypes may have caused changes in the observed dynamics.

The main goal of this work has been to reveal hidden patterns from the observed dynamics of the monthly incidence of rotavirus considering each serotype and all of them together. By hidden patterns, we mean information that is neither visually apparent nor extractable with conventional methods of analysis. Such conventional techniques include the tacit assumption of a linear system or stationarity, estimation of means, standard deviation and other features of histograms.

In this paper, we used several mathematical tools for this analysis: seasonal autoregressive integrated moving-average (SARIMA) models, power spectral density (PSD), higher-order spectral analysis (HOSA), such as bispectrum estimation and quadratic phase coupling (QPC), detrended fluctuation analysis (DFA), wavelet analysis (WA) and a surrogate data analysis technique. To our knowledge, HOSA and DFA have not been used previously to examine the dynamics of an epidemic. WA has been used to describe spatio-temporal waves in measles epidemics (Grenfell *et al.* 2001).

One of the purposes of this paper is to advocate the use of these relatively new techniques, such as HOSA, DFA and the wavelet transform (WT), for analysing the dynamics of epidemics.

The periodogram is a tool for analysing periodicities, i.e. it examines the frequency of different oscillations of the observed time-series. The periodogram is specifically designed for the detection of periodic patterns in a back-

ground of white noise (uncorrelated noise). The goal of spectral estimation is to describe the distribution (over frequency) of the power contained in a time-series, based on a finite set of data. Estimation of power spectra includes the detection of signals buried in white-band noise.

HOSA is useful for dealing with nonlinear time-series and for detecting interactions between harmonics (Swami *et al.* 1998). Most of the conventional methods are based on the power spectral analysis of the signal, so they are affected directly by the surrounding noises except in the rare cases where the ranges of power spectra of the noise from the signal to be analysed and the surrounding noise are separated completely, and they cannot use the quasi-periodical nature of the signal noise effectively. The use of the bispectrum overcomes these difficulties and is effective for detecting even such surrounding noises of the signal that appear only as the change of the relative phase among frequency components while keeping the amplitude of each frequency component unchanged (Stratonovich 1963; Rao & Gabr 1984).

The bispectrum is able to capture the phase information and to suppress the corruptive additive Gaussian noise, because the bispectrum is a statistical quantity which indicates the dependency among three frequency components whose frequencies $f_1$, $f_2$ and $f_3$ satisfy $f_1 + f_2 + f_3 = 0$; the bispectrum of any Gaussian noise vanishes completely (Stratonovich 1963).

The DFA technique is based on a modified root mean square analysis of a random walk, to assess the intrinsic correlation properties of a dynamic system separated from external trends in the data (Peng *et al.* 1994). DFA is a specialized time-domain technique, in which the time-series undergoes cumulative summing and then segmentation into short segments. Within each segment, the degree of dispersion of the cumulated time-series away from its linear trend is measured (as the sum of squares of residuals after subtracting the linear regression line). The total of the squared residuals for the individual segments is calculated for the overall dataset. The entire process is then repeated with a different segment length. Naturally, as the segments become longer, the degree of dispersion away from the linear regression line within the segments tends to increase. The rate at which this total dispersion increases as the windows become longer is measured as a slope, denoted by $\alpha$, on a log–log plot over particular regions of segment length. Steeper slopes are said to show higher complexity.

The formal application of the method of surrogate data (Theiler *et al.* 1992) is expressed in the language of statistical hypothesis testing. This involves two ingredients: a null hypothesis against which observations are tested and a discriminating statistic. The null hypothesis is a potential explanation that we seek to show is inadequate for explaining the data. If this statistic is different for the observed data that would be expected under the null hypothesis, then the null hypothesis can be rejected. The approach for detecting nonlinearity is to specify a well-defined underlying linear process or null hypothesis, and to determine the distribution of the quantity we are interested in for an ensemble of surrogate datasets which are just different realizations of the hypothesized linear stochastic process. In this paper, we use as a discriminating statistic the fractal scaling factors ($\alpha$s) obtained from the DFA.

The WT is devoted to the extraction of characteristic frequencies or specific oscillations, of a signal that, in our study, is composed of the monthly number of cases of rotavirus infection that includes four serotypes and the non-typeables plus the new serotype G9. The WT is a space–scale analysis which consists of expanding signals in terms of *wavelets* that are constructed from a single function, *the analysing wavelet* $\Psi$, by means of dilations and translations (Daubechies 1994). The WT is thus a cumulative measure of the variations of the signal (e.g. the monthly incidence of rotavirus) over a region proportional to the wavelet scale. Hence, the study of the behaviour of the wavelet values can reveal intrinsic properties of the dynamics that are masked by non-stationarity.

The paper is organized as follows. In each section we briefly describe the various methodologies and present their corresponding results. The interested reader is referred to Appendix A for some technical aspects of these methodologies.

We first describe the data and the surrogate data analysis technique. Second, we use the SARIMA technique to find an appropriate model to adjust the monthly incidence of rotavirus and to generate middle-term forecasts of the monthly incidence of rotavirus infections. Third, we detect the periodicities of the time-series by means of the periodogram and the bispectra. Fourth, we look for frequency and phase self-coupled harmonics in the incidence of rotavirus infection using HOSA. Fifth, we examine the correlation properties of the series using DFA and the surrogate data technique. Finally, we determine the scaling behaviour of the incidence of rotavirus by means of the WT and by the standard deviation of the wavelet coefficients as a function of the scale.

With the present analysis we characterize the overall dynamics of rotavirus infection and we conclude that essentially the inherent dynamics of rotavirus infection have not changed over time. The dynamics shows self-similar behaviour at different scales and it entails a multiple synchronization of the dynamics of each serotype.

We discuss the present results and their implications in the context of the biology of rotavirus infection.

## 2. SOURCES OF DATA

Data were obtained from diagnostic assays and from serotyping faecal rotavirus strains collected from children with severe diarrhoea admitted to the gastroenteritis ward of the Royal Children's Hospital (RCH) in Melbourne, Australia from 1977 to 2000. Serotyping data for the 1977–1988 (Bishop *et al.* 1991) and 1989–1993 (Masendycz *et al.* 1994) periods have already been published. Here, we present an overall mathematical analysis of all these data including the unpublished data of 1994–2000.

The total number of children attending the emergency department annually comprises all ages treated at this hospital, including newborn to 14 years. Most of the children admitted with acute gastroenteritis are under 3 years of age (Barnes *et al.* 1998). A decline in numbers over the whole period is not discarded owing to the introduction of peripheral suburban hospitals caring for children as out-

patients and inpatients. There is no reason to believe that the RCH would treat a disproportionate number of children with acute gastroenteritis.

The database includes 65 cases of the newcomer serotype G9, which appeared from 1999 to 2000.

The birth rate in Melbourne over the period of study remained stable. There were no demographic changes in the capture area or changes in the reporting system that would have influenced the results.

That there was a decrease in numbers of children presenting to the emergency department was due to the growth of peripheral hospitals, but the proportion of children admitted to RCH with rotavirus would not have been affected because preliminary studies have shown no bias in prevalence of rotavirus infection over the different Melbourne suburbs, including those served by RCH. Other sources of artefacts have been corrected by using the total figures for the emergency department.

The epidemiological data assembled over the 24 years would have not been influenced by changes in diagnostic techniques. From 1981, diagnosis of rotavirus infection relied predominantly on electron microscopy (EM). An 'in-house' enzyme immunoassay (EIA) was developed in the laboratory in 1977 and was in routine use from 1982 onwards.

Comparisons of this EIA with EM showed it to be slightly more sensitive. However, all specimens assayed by EM between 1977 and 1982 were collected at the height of rotavirus infection (within 48 h of admission) when it is not likely that EM would have failed to diagnose rotavirus infection. All serotyping has been done using the 'in-house EIA serotyping' assay developed in 1986. This assay has been used both retrospectively and prospectively after diagnosis of rotavirus positive specimens.

Figures used for all analyses included all rotavirus positive specimens and individual totals of specimens verified as containing serotypes G1, G2, G3, G4 and G9, and including additional non-typeable strains.

We used the software tools of MATLAB v. 5.3 and R12 for all the calculations. In general, differencing the data helped to clarify the estimates obtained with the different techniques that were used. All the *ad hoc* computer programs as well as the data can be downloaded at www.biomedicas.unam.mx/biolteor.

### (a) *Surrogate data analysis*

The surrogate data analysis technique was applied in order to discern if only random components or linear features of the incidence of rotavirus contribute to its dynamics.

We applied the method of Theiler *et al.* (1992) to transform the rotavirus time-series into surrogate time-series by means of the program 'chaos data analyzer' (Sprott & Rowlands 1995). Two different null hypotheses were tested to compare some statistics measured from both the original time-series and from their corresponding surrogate time-series.

(i) *Surrogate data type I*

Surrogate data are obtained by shuffling the original time-series of rotavirus, this is, by randomly changing their relative positions in the dataset, much like shuffling a deck of cards. The statistical moments (mean, variance, etc.) are preserved but all autocorrelations are destroyed, so that the surrogate time-series lacks any determinism. This shuffling suppresses any long-time correlations that may be present in the time-series that resides in the order of the data points. The null hypothesis is that *the incidence of rotavirus is a random process of independent random variables* and hence the difference between the original and surrogate datasets may be explained by a nonlinearly autocorrelated stochastic process.

If the statistics measured from the original rotavirus time-series turn out to be different from the ones measured from the surrogate time-series, then the null hypothesis that the statistics estimated from the original time-series come from an uncorrelated time-series is rejected (e.g. the original rotavirus time-series may be generated by deterministic mechanisms and the corresponding statistics would contain information about these mechanisms).

(ii) *Surrogate data type II*

To obtain a surrogate time-series where nonlinearities are destroyed, we applied the following procedure: the original time-series of the incidence of rotavirus is transformed by a discrete Fourier transform, the phases are randomized and the inverse discrete Fourier transform is calculated. The inverse Fourier transform is the surrogate data itself.

When phases are randomized, the nonlinearities that result from the interactions among phases in the original time-series disappear and the new surrogate time-series is a sum of only linear autocorrelations. If the statistics measured from the original rotavirus time-series were different from the ones measured from the surrogate time-series, then we reject the null hypothesis that *the incidence of rotavirus is a linear autocorrelated Gaussian process* (e.g. the original rotavirus time-series could contain nonlinear information that is captured by the estimated statistics).

In the surrogate hypothesis analysis we used the Student's $t$-test measured from the comparison of means between the original rotavirus time-series and from the average of 15 realizations of each type of surrogate time-series. The results are reported as mean ± standard deviation. The null hypotheses—that the original rotavirus incidence does not contain either deterministic or nonlinear components—were rejected only when the $p$-values were less than 0.001.

## 3. SARIMA MODELS

Many time-series contain a seasonal periodic component which repeats every $r$ observations. In the case of rotavirus, with monthly observations, where $r = 12$, we may typically expect $y_t$ (the number of cases of rotavirus at time $t$) to depend on terms such as $y_{t-12}$, and perhaps $y_{t-24}$, $y_{t-36}$, as well as terms such as $y_{t-1}$, $y_{t-2}$.... Box & Jenkins (1976) have generalized the autoregressive integrated moving-average (ARIMA) model to deal with seasonality, and define a general multiplicative seasonal ARIMA model (abbreviated SARIMA model) which can be found in Appendix A.

Detailed procedures for adjusting a particular SARIMA model can be found elsewhere (Box & Jenkins 1976; Shumway 1988). Briefly, when fitting a seasonal model to data, the first task is to reduce the series to stationarity and remove most of the seasonality.

The monthly incidence of rotavirus, including serotypes G1, G2, G3, G4 and G9 plus all non-typeables from 1977 to 2000, is shown in figure 1*a*. It can clearly be observed that the time-series exhibits an oscillatory behaviour. A detailed visual inspection of this oscillatory behaviour reveals annual epidemic cycles of low incidence that correspond to seasonal cycles, and various epidemic cycles of high incidence. It is also apparent that there is no obvious discernible pattern to the dynamics except for the annual cycle and that there is a wide variation in the size of the annual epidemics. Apparently, there is no regular behaviour of the prevailing serotypes of rotaviruses (not shown). There are also some months in which there are no registered cases of rotavirus infection, i.e. there are fade-outs in this time-series data.

It is also apparent that the rotavirus peaks in the last nine seasons are much higher than in all previous seasons. This difference in the amplitude of the annual oscillations makes the rotavirus time-series non-stationary, that is, its statistical properties change slowly or abruptly as a result of variations in background differences. To find the appropriate model, it is necessary to have a stationary time-series. Because there are large epidemic peaks in the original time-series a logarithmic transformation is reasonable. If the data are transformed to the first seasonal difference $z_a = y^* - y^*_{t-12}$, where $y^* = \ln y_t$, we get a stationary time-series. Since there are fade-outs we added to all months one case in order to make the logarithmic transformation.

To identify the particular time-series model that can be assumed to have generated the stationary time-series under consideration, we have to examine first the sample autocorrelation function (ACF) and the sample partial autocorrelation function (PACF) of the log-transformed stationary time-series. We use some general guidelines to identify which of the operators $\phi_p$, $\Phi_P$, $\theta_q$, $\Theta_Q$ should be used from the general seasonal multiplicative model to adequately represent our particular observed stationary time-series. The values of $p$, $P$, $q$ and $Q$ are to be assessed by looking at the ACF and PACF of the differenced series and choosing a SARIMA model whose ACF and PACF are of similar form. Finally, the model parameters are estimated by a standard iterative procedure. The order of the operators of the SARIMA model was suggested by the spikes (autocorrelations different from zero) of the sample ACF and the sample PACF which occur at lags substantially less than 12 months (not shown). Once the residuals of ACFs and PACFs are nearly zero (the residuals seem unrelated, i.e. the autocorrelation of the residuals is sufficiently small to lie within the bands of white noise) then that model offers a strong alternative to a plausible model.

In table 1 a summary of the parameter estimates of the model SARIMA $(1, 0, 0) \times (3, 1, 0)_{12}$ are presented together with their respective statistical values of significance. Note that the standard errors are small for each parameter and all the $p$-values are statistically significant. The absolute value of the $t$-statistics should be greater or equal than two in order to be statistically significant as is the case for each of the parameters. In figure 1*a* the fitting of this model to the monthly incidence of rotavirus is shown. This model shows an excellent agreement between the observed data and the predictions of the model. To gauge the performance of the best plausible model, we used the Akaike information criteria (AIC) (Akaike 1979) and the Bayesian information criterion (BIC) (Schwarz 1978). We tested several models such as: SARIMA $(1, 0, 0) \times (2, 1, 0)_{12}$ (AIC = $-0.61$; BIC = $-0.54$) and SARIMA $(1, 0, 0) \times (5, 1, 0)_{12}$ (AIC = $-0.67$; BIC = $-0.56$). These models also gave significant fittings to the data. However, the minimum values of both the AIC and BIC were obtained with the SARIMA $(1, 0, 0) \times (3, 1, 0)_{12}$ model (AIC = $-0.79$ and BIC = $-0.70$).

In figure 1*b* monthly incidence forecasts of the incidence of rotavirus together with their 95% confidence intervals are presented for the period 2001–2005. Note that the amplitude of the upper confidence interval increases with the forecasting time.

## 4. THE PERIODOGRAM

One way of estimating the power spectrum of a process is to find the discrete-time Fourier transform of the samples of the process (usually called fast Fourier transform (FFT)) and take the squared magnitude of the results. This estimate is called the periodogram (see Appendix A).

In figure 2*a* the PSD estimate (given in dB $Hz^{-1}$), i.e. the periodogram of the first differences of the monthly incidence of rotavirus is shown.

The main harmonics are numbered from 1–9. Note that the highest harmonic is the seasonal peak (number 1). The power of the harmonics that occur within a year (numbers. 2, 3 and 4) is greater than the power of the harmonics longer than a year (numbers 5–9). The harmonics 2, 3 and 4 correspond to periods of approximately six, four and three months, respectively. The harmonics 5, 6, 7, 8 and 9 correspond to periods of approximately 15, 23, 34, 64 and 213 months, respectively. The latter period of *ca.* 18 years seems to be a multiple of the 3-year period. It is clear from this periodogram that there are several harmonics other than the seasonal; the biannual and the quinquennial peaks. It also seems apparent that there is a negative linear relationship between the power and frequency for the peaks 1 to 4, whereas for the peaks 5, 6 and 8, and for the peaks 7 and 9, this relationship is positive.

The original time-series of the monthly incidence of rotavirus was randomized (surrogate type I) 15 times. The average slope of the power for this ensemble of surrogates was $0.0013 \pm 0.0007$. The log–log plot of the power spectrum of the incidence of rotavirus indicated that there were apparently three different slopes ($\beta$) (not shown). An estimate of the PSD for a single realization is shown in figure 2*b*. Note that the frequency spectrum of white noise is flat, because all frequencies are present in equal intensity (power) across the entire spectrum.

## 5. ESTIMATING CUMULANTS AND BISPECTRA

Linear systems are well behaved. The magnitude of their responses is proportionate to the strength of the stimuli. In addition, linear systems can be fully understood and predicted by dissecting out their components. The subunits of a linear system add up: there are no surprises or anomalous behaviours. By contrast, for nonlinear systems proportionality does not hold: small changes can have striking unanticipated effects. A further complication is that nonlinear systems cannot be understood by analys-

Table 1. Estimation of parameters of the model SARIMA $(1, 0, 0) \times (3, 1, 0)_{12}$.

| parameter | estimate | standard error | *t*-value | *p*-value |
|---|---|---|---|---|
| $\phi_1$ | 0.67 | 0.044 | 15.1 | 0.0 |
| $\phi_{1,12}$ | −0.72 | 0.058 | −12.39 | 0.0 |
| $\phi_{2,12}$ | −0.51 | 0.067 | −7.55 | 0.0 |
| $\phi_{3,12}$ | −0.31 | 0.06 | −5.21 | 0.0 |
| mean | 0.061 | 0.047 | 1.28 | 0.19 |
| constant | 0.051 | | | |

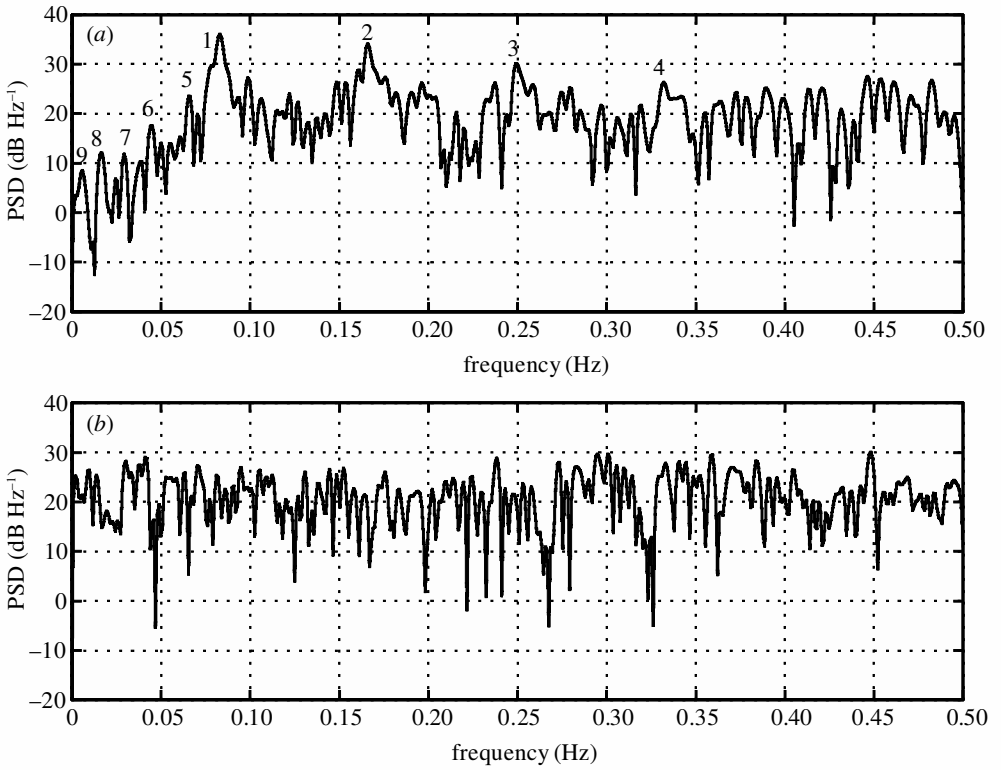


Figure 2. (*a*) Periodogram of the monthly incidence of rotavirus infection in Melbourne, Australia, 1977–2000. The duration of each of the numbered harmonics is as follows: (1) 12 months (0.08 Hz); (2) *ca*. 6 months (0.16 Hz); (3) *ca*. 4 months (0.25 Hz); (4) *ca*. 3 months (0.33 Hz); (5) *ca*. 15.6 months (0.06 Hz); (6) *ca*. 22.85 months (0.043 Hz); (7) *ca*. 33.7 months (0.029 Hz); (8) *ca*. 64 months (0.015 Hz); (9) *ca*. 213.3 months (0.0046 Hz). (*b*) Periodogram of the randomization of the original time-series.

ing their components individually. This reductionist strategy fails because the components of a nonlinear system interact, i.e. they are coupled. Their nonlinear coupling generates behaviours that defy explanations provided by traditional linear methods.

The use of the bispectrum is useful for detecting nonlinear systems of a time-series and for revealing the possible interactions of their components. The calculation of the bispectrum is based upon the estimation of the cumulants of the time-series.

Cumulants are nonlinear combinations of the moments of the process. The cumulants of a process are invariant to changes in the mean values of the process (see Appendix A).

The Wiener–Khinchin theorem states that the Fourier transform of the autocorrelation function equals the power spectrum (e.g. Shumway 1988). Similarly, the bispectrum is defined as the two-dimensional Fourier transform of the third-order cumulant, $C3(i, j)$ (Rao & Gabr 1984). The Fourier transform of the third-order cumulant, by itself, does not yield a consistent (reliable) estimate of the bispectrum. The estimate must be smoothed, either in the time domain (indirect method) or in the frequency domain (direct method). In this paper, the bispectrum of the data was estimated via the indirect method where the data were segmented into possibly overlapping records. We used a simple estimator of the bispectrum, the Fourier transform of the third-order cumulants of $\{c_{3y}(m, n)\}$, where $c_{3y}(m, n) = E\{y(t)y(t + m)y(t + n)\}$ (equation (A 4) of Appendix A (Swami *et al.* 1998)). Because of the symmetrical properties of the bispectrum (Rao & Gabr 1984), we present here only the first quadrant of the plane to display the bispectrum.

The contour plots of the indirect estimate of the bispectrum of the monthly incidence of rotavirus (first differences) for all serotypes, serotype G1, non-typeables, and the sum of serotypes G2 and G3, are shown in figure 3*a–d*, respectively.

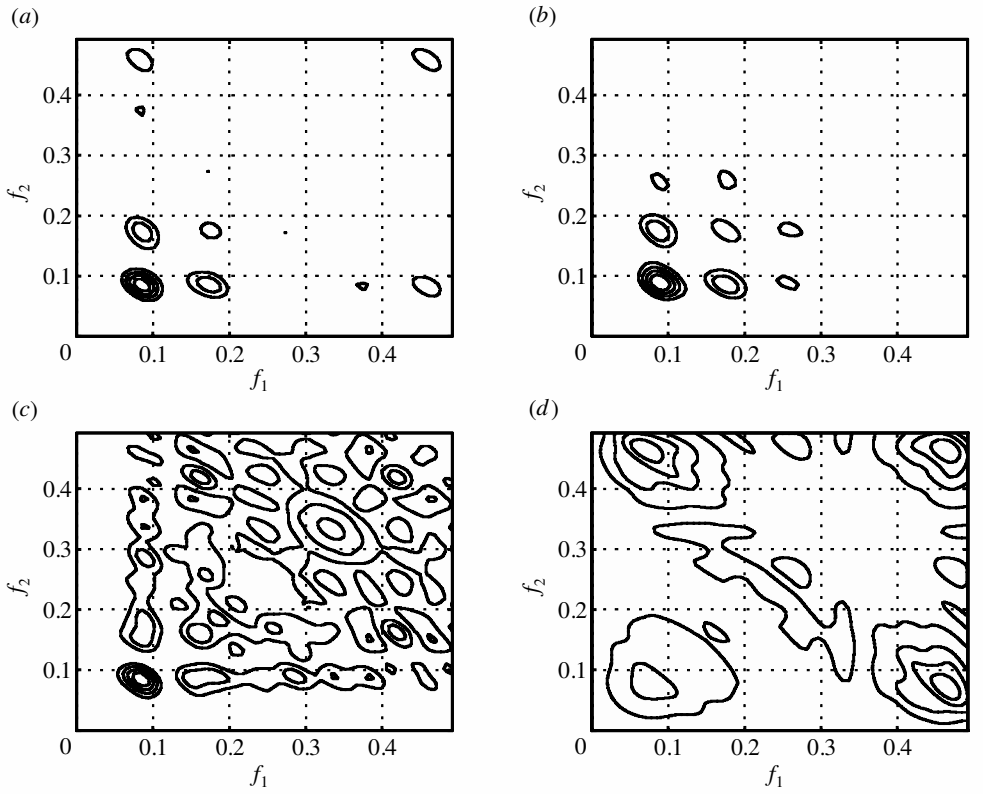


Figure 3. (*a*) Bispectrum of the monthly incidence of rotavirus (first differences) estimated by the indirect method; (*b*) bispectrum of serotype G1; (*c*) bispectrum of non-typeables; and (*d*) bispectrum of serotypes G2 and G3. Unbiased sample estimates of the third-order cumulants are computed for each record and then averaged across records; a lag window of 21 was applied to the estimated cumulants, and the bispectra were estimated as the two-dimensional FFT of the windowed cumulant function (see equation (A 3)).

Both the direct (not shown) and the indirect method estimates of the bispectrum of all serotypes, serotype G1 and non-typeables reveal sharp peaks at (0.08, 0.08). Soft harmonics can be seen for all serotypes and for serotype G1 at (0.16, 0.16). The bispectrum of serotype G1 is similar to the bispectrum when all serotypes are included. The presence of pronounced peaks in the bispectrum is indicative of nonlinear phenomena. Thus, these harmonics indicate that there are nonlinearities in the time-series and, therefore, there may be possible quadratic coupling. This test confirms that the data are non-Gaussian, and shows evidence of a fundamental period of *ca*. 1 year plus a harmonic of approximately six months (when all serotypes are included).

The non-typeables show a sharp peak at (0.08, 0.08) and soft harmonics at all frequencies. The bispectrum of serotypes G2 and G3 does not show an annual harmonic but interestingly it shows soft harmonics at low, intermediate and high frequencies. The soft harmonics observed in the non-typeables and in the sum of G2 and G3 disappear when all serotypes are included. Then, when all rotavirus infections are included, an emergent pattern arises coming from the nonlinear interactions of the different serotypes.

## 6. PARAMETRIC BISPECTRA AND QPC

Phase coupling occurs because of nonlinear interactions between harmonic components. If there exist triplets $\{f_1, f_2, f_3\}$ and $\{\phi_1, \phi_2, \phi_3\}$ so that $f_1 + f_2 = f_3$ and $\phi_1 + \phi_2 = \phi_3$, we say that the signal exhibits quadratic frequency and phase coupling, respectively. The presence of quadratic or cubic phase-coupling cannot be detected using the autocorrelation function, but they can be detected and quantified using the third- and fourth-order cumulants (Appendix A).

Bispectra have shown promise in these applications because frequency and phase coupling indicate nonlinear interactions among harmonic components (Priestley 1988; Swami *et al.* 1998).

QPC, coupling at sum and differences of frequencies, occurs when a signal is passed through a square-law device, for example, and may be detected from the bispectrum (Priestley 1988). The general theory of Volterra systems is used for describing these nonlinear interactions (Appendix A).

Less attention has been paid to what is referred to as self-coupling which amounts to the presence of pairs $\{f_1, f_1 + f_1\}$ and $\{\phi_1, \phi_1 + \phi_1\}$ in the quadratic case. In the case of self-coupling (Tick 1961; Zhou & Giannakis 1994), the bispectrum can be used to verify the presence of higher-order couplings as well. To our knowledge, the possibility of self-coupling has not been investigated in the case of an epidemic.

To check for QPC, we estimated the parametric bispectrum via the subroutine *qpctor* of MATLAB v. 5.3 (Swami *et al.* 1998). This subroutine is based upon the nonlinear Volterra model (see Appendix A). With a single realization we used an autoregressive order of eight to estimate the parametric bispectrum.

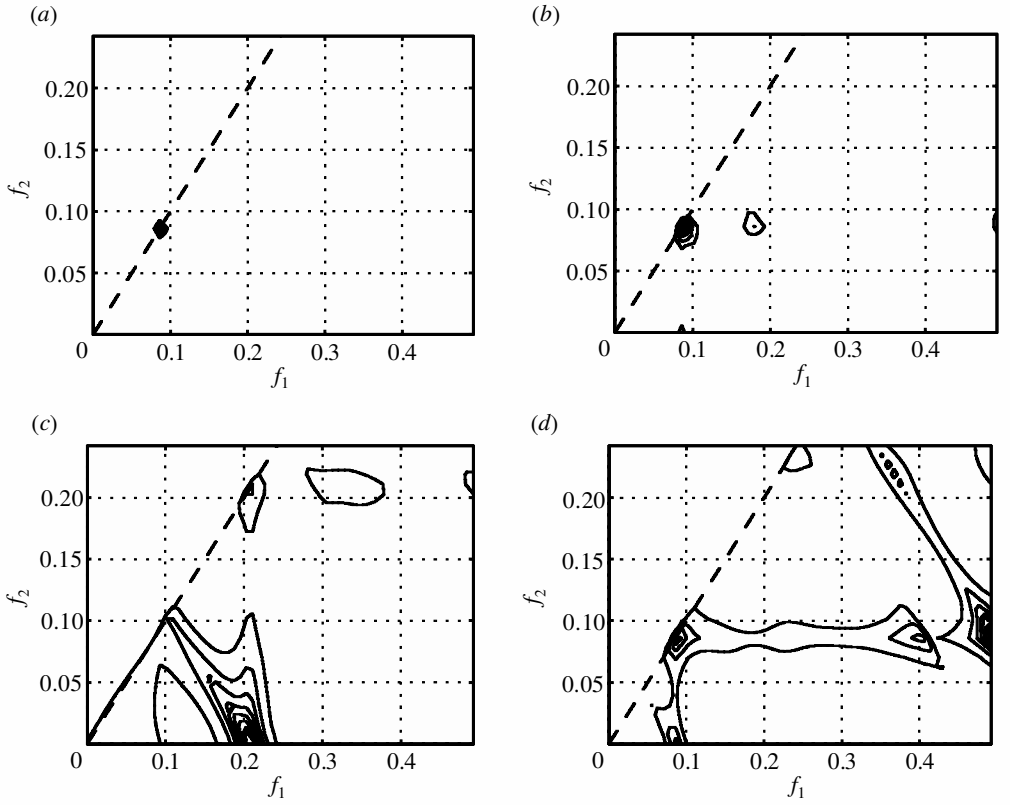


Figure 4. (*a*) The parametric bispectrum of the monthly incidence of rotavirus considering all serotypes for the period 1977–2000 (300 months); (*b*) the parametric bispectrum considering all serotypes for the first 224 months; (*c*) the parametric bispectrum for the uncorrelated time-series; and (*d*) the parametric bispectrum when the phases are randomized. Note that in (*a*), (*b*) and (*c*) there is a QPC of the annual cycle ($f_1 + f_1 = 0.16$) which means that the annual cycle interacts with itself so that it is quadratically phase coupled with the six-month cycle.

In figure 4*a*,*b*, the estimated parametric bispectra of the rotavirus data for the period 1977–2000 and for the first 224 months both show a contour plot that occurs at $f_1 = f_2 = 0.08$.

This is the region which is formed by the quadratic coupling of two harmonics. Because $f_1$ and $f_2$ lie in the straight line of 45° then they are equal. This means that the seasonal cycle interacts with itself so that we have a self-exciting frequency and phase coupling that produces nonlinearly (quadratically) the harmonic of six months. We chose the period of 224 months because it does not include the apparently different dynamics of the last years. For shorter periods of time the QPC still prevails but spectral leakage (noise that arises from short time-series) becomes more prominent. We also estimated the parametric bispectrum for each serotype and for certain combinations of them (not shown). None of the serotypes or partial combinations of them showed QPC. *QPC occurred only when all serotypes were included. Thus it seems that a multiple synchronization of all serotypes is needed for QPC of the annual cycle to occur.*

In figure 4*c*,*d* the corresponding parametric bispectra of single realizations of surrogate type I (uncorrelated series) and surrogate type II (nonlinearities are destroyed) are illustrated. Note that the clear-cut rhombi representing the QPC of the original time-series disappears in both cases.

## 7. DFA

A system is said to exhibit long-range correlations when some physical properties of the system are correlated at different times and the corresponding correlation function decays much slower than exponentially as a function of time. Usually, long-range correlations are a result of the collective behaviour of a complex system (under unique conditions), with the multiple components interacting through local (short-range) interactions. The moments of the distribution of a time-series do not contain information about the dynamics of the epidemic process. The DFA permits the detection of long-range correlations embedded in a seemingly non-stationary time-series and also avoids the spurious detection of apparent long-range correlations that are an artefact of non-stationarity.

With white noise, no correlations exist in the time-series, and the series is completely random. Alternatively, there may be short-range correlations in the time-series that decay rapidly as the data points move further apart. This type of short range correlation is very common in nature. One extreme example is the so-called random walk or Brownian noise. In this case, the signal at any given instant is strongly correlated to the previous interval. The frequency spectrum for a random walk process is characterized by a rapidly decaying smooth curve in which the amount (power) of the fluctuation is inversely pro-

portional to the frequency squared ($1/f^2$). The exponent 2 in this power-law relationship between frequency and power is called the scaling exponent $\beta$.

Another type of noise that is commonly encountered in nature exhibits persistent long-range correlations (Peng *et al.* 1993), i.e. the value at every point is partially dependent on the values at all previous points. This is called $1/f$ noise. The frequency spectrum is also a smooth curve, but the amplitude of fluctuations is inversely proportional to the first power of frequency ($1/f$, $\beta = 1$), obeying the $1/f$ power law of fractal-like processes (Shlesinger 1987). $1/f$ noise is usually associated with the dynamic behaviour of time-series generated by complex systems that have multiple time-scales.

A detailed description of the DFA method is presented in Appendix A. Typically, the root-mean square fluctuation of the integrated and detrended time-series is represented by the function, $F(n)$, that will increase with box size $n$. A linear relationship on a double log graph indicates the presence of scaling. Under such conditions, the fluctuations can be characterized by a scaling exponent $\alpha$ (self-similarity parameter), the slope of the line relating $\log F(n)$ to $\log n$.

If the data are uncorrelated, the integrated value, $y(k)$, corresponds to white noise, and therefore $\alpha = 0.5$ (Montroll & Shlesinger 1984). If there are only short-term correlations, the initial slope may be different from 0.5, but $\alpha$ will approach 0.5 for large window sizes. In the language of random walks, for $\alpha = 0.5$ there is no bias and the random walker is equally likely to step in either direction no matter what the last step was. An $0.5 < \alpha < 1.0$ indicates persistent long-range power-law correlations such that a large (compared to the average) incidence interval is more likely to be followed by a large interval and vice versa. For $0.5 < \alpha < 1$ the walker has a tendency to continue in the direction they are going, so there is persistence of the process; given a step in a particular direction that step is remembered and the likelihood of the next step being in the same direction is greater than that of changing directions. By contrast, for an $0 < \alpha < 0.5$, indicates a different type of power-law correlation such that large and small values of the time-series are more likely to alternate. Analogously, for $0 < \alpha < 0.5$ the random walker prefers to change their mind with each step, so there is anti-persistence; given a step in a particular direction that step is remembered and the likelihood of the next step being in the same direction is less than that of reversing directions. A special case of $\alpha = 1$ corresponds to $1/f$ noise (Shlesinger 1987). For $\alpha \geqslant 1$, correlations exist but cease to be of a power-law form; $\alpha = 1.5$ indicates brown noise, the integration of white noise. The $\alpha$ exponent can also be viewed as an indicator that describes the 'roughness' of the original time-series: the larger the value of $\alpha$, the smoother the series. In this context, $1/f$ noise can be interpreted as a compromise or balance between the complete unpredictability of white noise (very rough landscape) and the much smoother landscape of Brownian noise (Peng *et al.* 1995).

For statistically robust results very long datasets are required. For practical purposes, epidemiological researchers are often interested in the possibility of using substantially shorter time-series.

In figure 5 the results of the DFA to both the actual data of rotavirus incidence (diamonds) and the SARIMA $(1, 0, 0) \times (3, 1, 0)_{12}$ model (asterisks), as well as the resulting DFA of single realizations of a surrogate type I (dashed line) and surrogate type II (dot–dashed line) are shown. The DFA of the model behaved essentially the same as the actual data.

A good linear fit of the log $F(n)$ versus log $n$ plot should be proportional to $n^{\alpha}$, where $\alpha$ is the single exponent describing the correlation properties of the entire range of time-scales. However, in some of the scales we found that the DFA plot was not strictly linear but rather consisted of three distinct linear regions of different slopes separated at two breakpoints, $n$BP1 and $n$BP2. This observation suggests that there is a short-range scaling exponent, $\alpha_1$, over a period from $n = 4$ months up to $n$BP1 (*ca.* 12 months), a long-range scaling exponent, $\alpha_2$, from $n$BP1 to $n$BP2 (*ca.* 36 months), and another long-range exponent, $\alpha_3$, from $n$BP2 up to 64 months.

In brief, we note that for the rotavirus time-series DFA detects two crossovers, namely, within a year there is one behaviour where $\alpha_1 = 1.08$ ($1/f$ noise), between 1 and *ca.* 3 years there is another behaviour where $\alpha_2 = 0.23$ (indicating anti-persistent power-law correlations) and, between 3 and *ca.* 5 years $\alpha_3 = 0.64$ (which means that there are persistent long-range power-law correlations).

To rule out the possibility that these three different scaling factors could be the result of an artefact the surrogate data technique was applied. Fifteen realizations of surrogate type I and type II were carried out. The average value of the single slope obtained for the ensemble of surrogates type 1 was: $\langle\alpha\rangle = 0.504$. The average values of the three slopes for the ensemble of surrogates type II were $\langle\alpha_1\rangle = 0.58$; $\langle\alpha_2\rangle = 0.06$ and $\langle\alpha_3\rangle = 0.06$. The corresponding standard deviations were: $\sigma_1 = 0.074$; $\sigma_2 = 0.019$ and $\sigma_3 = 0.024$. The three $p$-values are so small ($p_{\alpha_1} = 3.5 \times 10^{-13}$; $p_{\alpha_2} = 8.6 \times 10^{-15}$; and $p_{\alpha_3} = 0$) that sufficient evidence has been gathered to reject the null hypothesis that the three observed $\alpha$s could be the result of an artefact.

## 8. WT

Unlike Fourier, WT is usually devoted to the analysis of non-stationary and nonlinear signals. Traditional approaches (such as the power spectrum and correlation analysis) are not suited for such non-stationary sequences, nor do they carry information stored in the Fourier phases which is crucial for determining nonlinear characteristics.

Thus there is no prerequisite over the stability of the frequency content along the signal analysed. Conversely to Fourier, WA allows one to follow the temporal evolution of the spectrum of the frequencies contained in the signal. The shape of the WT-analysing wavelet equation differs from the fixed sinusoidal shape of the Fourier transform and can be designed to better fit the shape of the analysed signal, allowing a better quantitative measurement.

Like Fourier or Laplace transforms, the continuous wavelet transform (CWT) is an integral transform. WA can be considered as a local Fourier analysis performed at different separated levels. A formal definition of the CWT is given in Appendix A.

The analysis amounts to sliding a window of different weights (corresponding to different levels) containing the wavelet function all along the signal. The weights characterize a family member with a particular dilation factor.

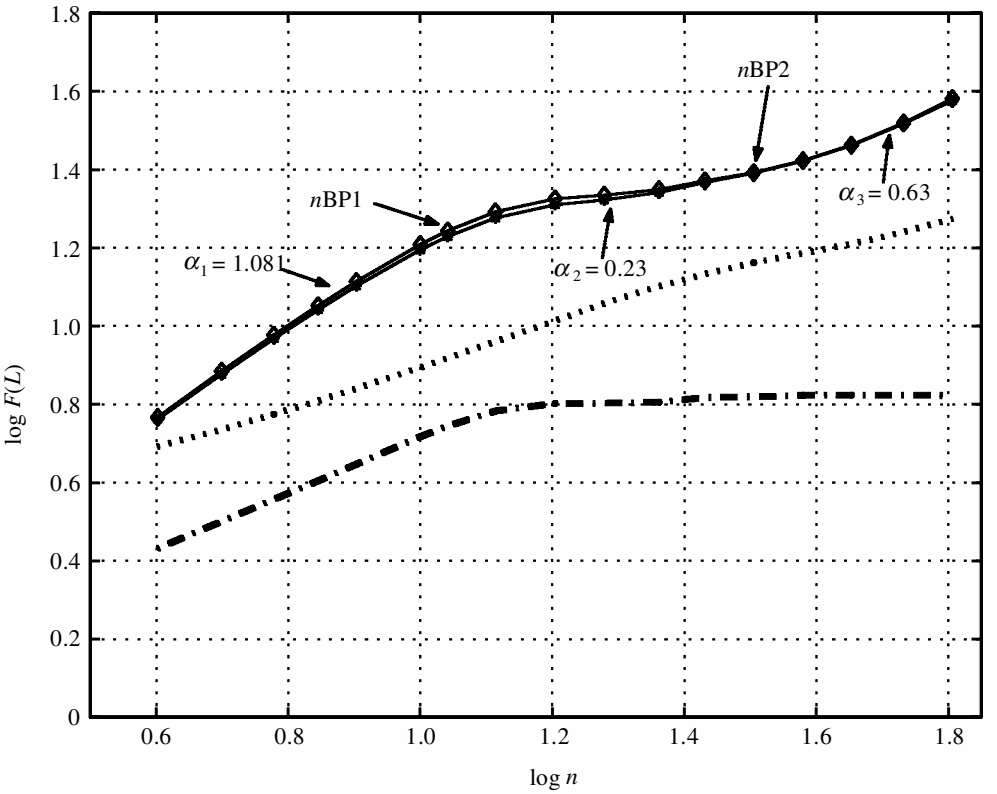


Figure 5. Detrending fluctuation analysis. Plot of log $F(n)$ versus log $n$ for the incidence of rotavirus from 1977 to 2000 (300 months). Arrows indicate crossover points $n$BP1 and $n$BP2 that form three different regions in scaling. The α exponents for each of the three different regions are: $\alpha_1 = 1.08$; $\alpha_2 = 0.23$; $\alpha_3 = 0.64$. Diamonds, actual data; asterisks, SARIMA $(1, 0, 0) \times (3, 1, 0)_{12}$ model. The DFA of single realizations of surrogate type I (dotted line) and surrogate type II (dash–dotted line) are also shown.

Thus the wavelet coefficients correspond to the scalar product of the given signal $S$ with the wavelets $\Psi_{a,b}(t)$ obtained by dilating ($a$) and translating ($b$) the *analysing wavelet* $\Psi(t)$. In other words, the WT $T$ gives a serial list of coefficients called the wavelet coefficients and represents the evolution of the correlation between the signal $S$ and the chosen wavelet at different levels of analysis (or different ranges of frequencies) all along the signal $S$.

The WT $T$ is sometimes called a mathematical microscope or telescope because it allows the study of the properties of the signal on any chosen scale $a$. For high frequencies (small $a$), the $\Psi$ functions have good localizations (being effectively non-zero only on small sub-intervals), so short-time regimes or high-frequency components can be detected by WA.

We have done the CWT using a broad range of orthonormal, compactly supported analysing wavelets (Misiti *et al.* 2000). We present results for the reverse biorthogonal wavelet pairs: rbioNr.Nd. The order is represented by Nd and Nr (d for decomposition and r for reconstruction). We chose this analysing wavelet because the shape of both its reconstruction and decomposition wavelet functions (psi-scaling functions), resemble the short-term oscillatory behaviour of the first differences of the monthly incidence of rotavirus. However, similar results were obtained using other wavelets such as Haar and coiflet 2 (not shown).

In figure 6 the CWT of the rotavirus incidence using as an analysing wavelet the reverse biorthogonal spline with Nr = 1 and Nd = 3 (rbio1.3) is shown.

Note that every year there are three rhombi of similar size throughout 64 scales indicating self-similarity of the signal. It is also evident that there is a symmetrical pattern of the CWT over time. In particular, note that there are two types of uninterrupted dark diagonal straight lines: some diagonals increase over time, from small scales to large scales, whereas other diagonals decrease over time, from large scales to small ones. The resulting pattern is that of several repetitive triangles consecutively formed over time. Some of these triangles have their bases at high frequencies (small scales), whereas in others their bases occur at very low frequencies (large scales). Note also that these triangles are part of the three rhombi formed every year, and of the rhombi formed every 2 and 3 years. Because the darker colours indicate the smallest values of the wavelet amplitudes, the dark diagonals represent the distribution of 61 fade-outs of the original time-series over time and for all scales. The emerging successive and symmetrical triangles that arise from this distribution of fade-outs constitute the skeleton of the whole pattern of the resulting WT. The transmission of rotavirus infection seems to be a multiplicative process, following a power-fractal scaling repelled from these fade-outs. Each year there are bright vertical lines that cross all scales and that arise from the vertex of some of these triangles at very low frequencies. This vertical lines show certain vibration that may be associated with the annual self-exciting QPC. *The whole pattern is the same throughout all the period analysed (1977–2000) regardless of the specific sequence of presence (or absence) of a particular serotype.* This self-similar pattern

becomes more apparent during the last 6 years. Then because certain wavelets $\Psi$ have vanishing moments, polynomial trends in the non-stationary signal are automatically eliminated in the process of wavelet transformation (Daubechies 1994). This is salutatory in the case of the rotavirus epidemics, as is evident from the trends apparent in figure 1*a*, which are eliminated by the WT shown in figure 6.

### (a) *Standard deviation of wavelet coefficients as a function of the scale*

Orthogonality in the CWT ensures that the information represented at a certain scale $a$ is disjointed from the information of other scales. Because the signal $S$ fluctuates in time, so too does the sequence of wavelet coefficients at any given scale, though its mean is zero (Daubechies 1994). A natural measure for this variability is the wavelet-coefficient standard deviation, as a function of scale:

$$\sigma_{\mathrm{wav}}(a) = \left[ \frac{1}{Nc - 1} \sum_{n=0}^{Nc-1} [T_{a,n}(s) - \langle T_{a,n}(s) \rangle]^2 \right]^{1/2},$$

where $N$c represents the number of wavelet coefficients at a given scale $a$.

In figure 7 the graphs of the standard deviation of the wavelet coefficients, $\sigma_{\mathrm{wav}}$, of the analysing wavelet (rbio1.3) against the scale ($1 \leqslant a \leqslant 64$) for the actual data (diamonds), the SARIMA $(1, 0, 0) \times (3, 1, 0)_{12}$ model (asterisks), as well as for serotypes G1, G2 and G3, G4, and non-typeables are each pointed out with an arrow.

Note first that the agreement between the data that includes all rotavirus infections and the model is remarkable. Note also that the standard deviation of the magnitude of the coefficients shows three cycles as the scale increases (frequency decreases and period increases). Most of the variation in the magnitude of the coefficients occurs within a year (scales 0 to *ca*. 24). The other two cycles occur at longer periods than a year. The variation of these longer cycles ranges from scales *ca*. 24 to *ca*. 48, and from *ca*. 48 to 64. For each cycle the maximum variation diminishes as the scale increases (frequency decreases). Note that these three cycles correspond to the three different slopes ($\alpha_1$, $\alpha_2$, $\alpha_3$) obtained by the DFA. The same oscillatory behaviour is observed for serotypes G1 and non-typeables. The sum of serotypes G2 and G3 shows variation only for the annual cycle but not for longer cycles. The annual standard deviation of wavelet coefficients of serotype G4 is small and roughly constant from scales approximately 20 to 64.

## 9. DISCUSSION

In this work we have used several mathematical techniques to characterize the overall dynamics of the rotavirus epidemics. Although SARIMA, PSD, HOSA, DFA and WA are related techniques (e.g. Heneghan & McDarby 2000), each of them revealed differently hidden dynamical aspects of the rotavirus epidemic. It is important to remark that we used a very short time-series of the rotavirus epidemic ($N = 300$ months). The most noteworthy findings of the present analysis are as follows.

(i) Time-series analysis has been used to examine oscillatory secular trends of the monthly incidence of rotavirus in Melbourne, Australia for the period of 1997–2000. A SARIMA $(1, 0, 0) \times (3, 1, 0)_{12}$ model tested by order determination criteria adequately describes the monthly incidence of all rotavirus infections (§ 3). This statistical model was also used to produce middle-term forecasts of the monthly incidence of the epidemic.

(ii) We have examined the statistical evidence for regularity in the epidemic cycles of rotavirus. In particular, a periodogram was used to determine the periodicities of the epidemic. Seasonal, biannual and quinquennial periods were found (interepidemic cycles). However, we also detected a fundamental period of 3 years that turned out to be a dominant component of the series as it was reflected in the SARIMA $(1, 0, 0) \times (3, 1, 0)_{12}$ model (§ 4).

(iii) We used HOSA to calculate the bispectrum and we observed that the time-series is nonlinear and it suggested nonlinear interactions between harmonics. We also confirmed that the time-series is non-Gaussian (§ 5). The bispectra of serotype G1 and non-typeables clearly displayed a sharp annual harmonic but that was not the case with the bispectrum of the sum of serotypes G2 and G3. Therefore, there should be nonlinear interactions among the dynamics of all serotypes. In other words, the whole is not equal to the sum of its parts.

(iv) We used HOSA to show that in the rotavirus epidemic there is both frequency ($2f_{\mathrm{annual}} = f_{\mathrm{six\ months}}$) and phase self-coupling ($2\phi_{\mathrm{annual}} = \phi_{\mathrm{six\ months}}$) of the annual cycle that generates a six-month cycle. This result is astounding given the great heterogeneity of the incidences of each serotype of rotavirus. The same self-coupling was obtained using data of the first 224 months since 1977. This means that the inherent dynamics has not changed. Only the amplitude of the cycles has changed. The dynamics of each serotype is multiple synchronized in such a way that they behave as a single unit at the epidemic level (§ 6).

(v) The whole dynamics follows a scale-free power-law fractal scaling behaviour as shown by DFA. By means of DFA we demonstrated that there may be two breakdowns in the fractal scaling of the incidence fluctuations of rotavirus. Therefore, these three scaling regions in the time-series suggest that processes influencing the epidemic dynamics of rotavirus over less than 12 months differ from those that operate between 1 and *ca*. 3 years, as well as those between 3 and *ca*. 5 years (§ 7). By means of a surrogate data technique we were able to discard the possibility that the three observed different scaling regions may be the result of an artefact.

(vi) We showed that it is possible to characterize the scaling behaviour of the epidemic of rotavirus by using wavelets. The CWT of the monthly incidence of rotavirus reflected clearly the annual self-similar behaviour of the epidemic as predicted by the DFA analysis. The annual wavelet coefficients displayed three similar rhombi at different ranges of the scale. Similarities were also found following the global behaviour of the epidemic. We detected the formation of successive triangles over time (§ 8).

(vii) We found that there are three main cycles that characterize the whole of the epidemic and that each of these cycles corresponds to the three different scaling regions as detected by DFA. There is a considerable variation throughout these three scaling cycles as reflected by the standard deviation of the magnitude of wavelet coefficients which decreases as frequency decreases (§ 8a). Serotype G4 and the sum of cases associated with serotypes G2 and G3 showed variations only within the annual cycle.

Given that the rotavirus peaks in the last nine seasons are much higher than in all previous seasons, we initially put forward the hypothesis that there could be a change in the dynamics. Because the underlying dynamics is the same throughout all the analysed period, the increase in amplitude of the last years may be due to the fact that the criteria for admission to hospital changed 9 years ago due to the introduction of oral rehydration therapy. This meant that more children with acute gastroenteritis were treated as day-care patients and were not admitted to hospital for treatment. Only the really severe cases were admitted to hospital, and these would have included a higher proportion of rotavirus infected children, as this pathogen causes comparatively more severe symptoms than the other enteric pathogens in this age group.

The incidence of rotavirus epidemics fluctuates apparently in a complex manner. The intrinsic importance of the SARIMA model lies not for the precise numerical values but in developing a first step to understand the processes underpinning this epidemic and to anticipate a likely scenario of the behaviour of the epidemic in Melbourne, Australia for short- and middle-term time-scales. This model provides an explanation for the observed crossover behaviour of the data (figure 5), and it suggests that three inputs dominate the system at different time-scales: one in which each value is partially dependent on the values at all previous points ($1/f$ noise), and each of the other two, with long-range correlations. The model also showed QPC due to quadratic terms of the model (not shown).

The annual cycles seem to arise from seasonal climatic changes and the six-month cycle is related to the whole winter period. Seasonal variation in the transmission rates can generate biennial epidemics but seasonality seems not to be the necessary condition that accounts for the driving force of longer interepidemic cycles. The biannual and triennial periods are most likely to be connected with the age-distribution of cases (José *et al.* 1996). It particular, it has been shown that the biannual period is directly related to the average age at which susceptible individuals acquire the rotavirus infection (José *et al.* 1996). Rotavirus infections have been shown to occur in all age groups and are particularly common in adult members of families of children with rotavirus-associated diarrhoea (Bishop 1994). The potential importance of reinfections in adults is that they can serve as reservoirs to maintain rotavirus in the community and assure its circulation to susceptible individuals. It is possible that the long interepidemic cycles may be associated with the dynamics of asymptomatic carriers, often older siblings and parents of young children (Velazquez *et al.* 1993; Bishop 1994). The *ca.* 5 and *ca.* 6 year period cycles seem to be associated with changes over time of the phases of the epidemic that may have to do with the spread of the infection, probably from a core group to smaller groups. This in turn may be related to the spatial propagation of the disease from the central city of Melbourne to several suburbs.

Higher-order cumulants and the parametric bispectrum were useful to isolate specific types of self-coupling. There seems to be a synchrony among serotypes that preserves a particular dynamical pattern despite the apparent changes in the seroprevalence of the last years. The intrinsic dynamics is unaltered by the emergence of new serotypes, the re-emergence of old serotypes or the transient disappearance of a particular serotype (see figures 2*a*,*b*, 3, 5 and 6).

The mechanisms underlying the observed long-range power-law correlations appear to be related primarily to countervailing inputs. There seem to be, on the one hand, factors that decrease the firing rate of the epidemic, and on the other hand there seems to be something that has the opposite effect (presumably related to changes in the immunological resistance of the hosts). The nonlinear interaction (competition) between these forces may be a probable mechanism that maintains the epidemic. Fractal curves are known to be scale invariant, which means that the statistical properties of the signal remain invariant under scale transformations.

Scale-free power laws governing epidemics have recently been described in the measles records for small isolated populations (Rhodes & Anderson 1996) and for the web of human sexual contacts (Liljeros *et al.* 2001).

Given that the incidence of rotavirus follows a power-law fractal behaviour, its cumulative distribution (not shown) consists of a hierarchy of small but highly frequent epidemics followed by less frequent large epidemics, although their occurrence is connected and governed by scaling exponents.

Power laws rarely emerge in systems completely governed by the roll of a die. Most often they signal a transition from disorder to order. Power laws are typical of self-organization in complex systems.

The possibility of the presence of a group of individuals inherently more susceptible to acquire or to transmit the rotavirus infection must be arbitrary because there is no well-defined boundary that separates the group of high spreaders from other individuals.

It is reasonable to assume that each of the regulatory systems that participate in the rotavirus incidence has a preferred frequency of operation; the absence of a characteristic time-scale within a year may be taken to imply that no single regulatory system dominates the regulation of the epidemics of rotavirus. The observed $1/f$ seasonal pattern of rotavirus epidemic could simply be a mirror of a limit distribution, to wit, the lognormal distribution. This implies that one should seek mechanisms that have a multiplicative rather than an additive nature. Mechanisms that can account for the transition of distributions having finite central moments such as the lognormal, to inverse power-law distributions have been proposed (West & Shlesinger 1989). Although the fractal organization of the annual cycle of rotavirus epidemic is not understood, it may represent a network of coupled pathways and feedback loops that regulates the annual cycles and thus permits rapid adaptation to the host–parasite interactions.

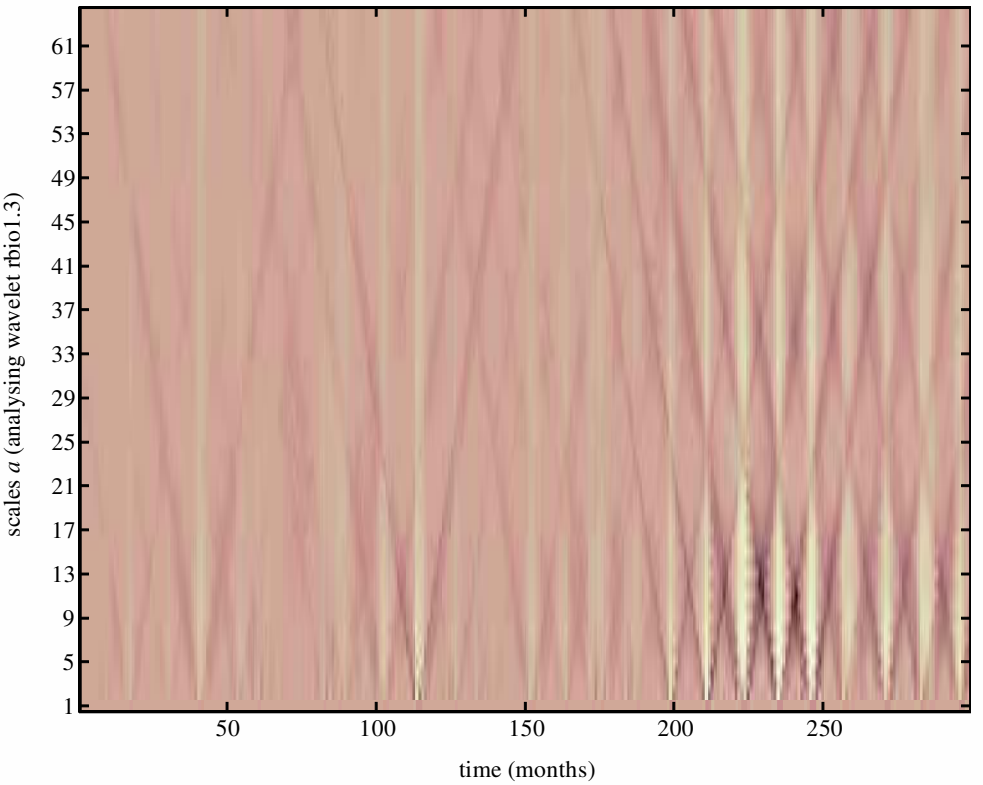


Figure 6. Colour-coded CWT of the incidence of rotavirus. The *x*-axis represents time (300 months) and the *y*-axis indicates the scale of the wavelet used ($a = 1, 2, \ldots, 64$) with large scales (low frequency) at the top. The brighter colours indicate larger values of the wavelet amplitudes. The WA was performed with the reverse biorthogonal spline with $Nr = 1$ and $Nd = 3$ as an analysing wavelet and it uncovers a hierarchical scale invariance quantitatively expressed by the stability of the scaling form. This wavelet decomposition reveals a self-similar fractal structure in the incidence of rotavirus every year, i.e. there are three rhombi of similar shape at different ranges of the scale. The CWT also unravels a repetitive pattern of successive triangles that are formed over time.

The resemblance of the wavelet pattern upon magnification reproduced the whole structure. The CWT of each serotype and certain combinations of them, reflected a roughly similar pattern to that obtained with all serotypes, particularly the formation of the apparent triangles (not shown), i.e. each serotype behaved essentially in a similar fashion as the whole. However, the wavelet of each serotype did not show the bright vertical line crossing all scales. This is consistent with the observation that QPC was not obtained for any serotype in particular, and that annual fractal scaling does not lead by itself the annual self-QPC. It is evident that the integration of the dynamics at different scales of all serotypes is the result of QPC. It may appear that the different serotypes act synchronously in relays.

No central serotype sits in the middle of the epidemiological distribution. There is no single serotype whose removal could break the epidemic. This means that not all severe cases can be associated with a single particular rotavirus serotype that uniquely can lead to acute gastroenteritis. In other words, the power-law behaviour and the self-similar pattern observed by the WA imply that there is no such thing as a universal intrinsically more virulent rotavirus strain. It is not a surprise then that studies carried out in different continents and during diverse time periods have reported different more virulent serotypes related to severe gastroenteritis (Bern *et al.* 1992; Cascio *et al.* 2001). Our results are consistent with differences in the relationship serotype–illness severity observed among different geographical areas (Bern *et al.* 1992; Cascio *et al.* 2001).

The clinical outcome during a rotavirus infection may be determined by a prolonged absence of a given serotype, i.e. a serotype which has not circulated in the population for a sufficiently long period of time, for which the population may become immunologically susceptible.

Because the characteristics of this fractal evolve with time and become local, then this is consistent with a multifractal dynamics of the incidence of rotavirus. Because at least three different exponents are required to characterize the scaling properties of the signal fully (as observed both in the DFA analysis and in the periodogram), then the overall dynamics of the epidemic is consistent with a multifractal character. Multifractals can result from random multiplicative processes. There are two major differences between the behaviour of multiplicative and additive random processes. For multiplicative processes, a rare event can dominate the distribution, whereas for additive processes, rare events have little impact. The result is that the multiplicative processes have distributions with long tails. Also, in a multiplicative process, short-range correlations can have a strong impact, whereas additive processes are insensitive to short-range correlations because correlated pairs are often distributed as if they were a single random variable. Then the general features of multifractals are consistent not only with the results of the DFA (hence with $1/f$ noise), but also with the SARIMA model and the resulting WT. The wavelet approach suc-

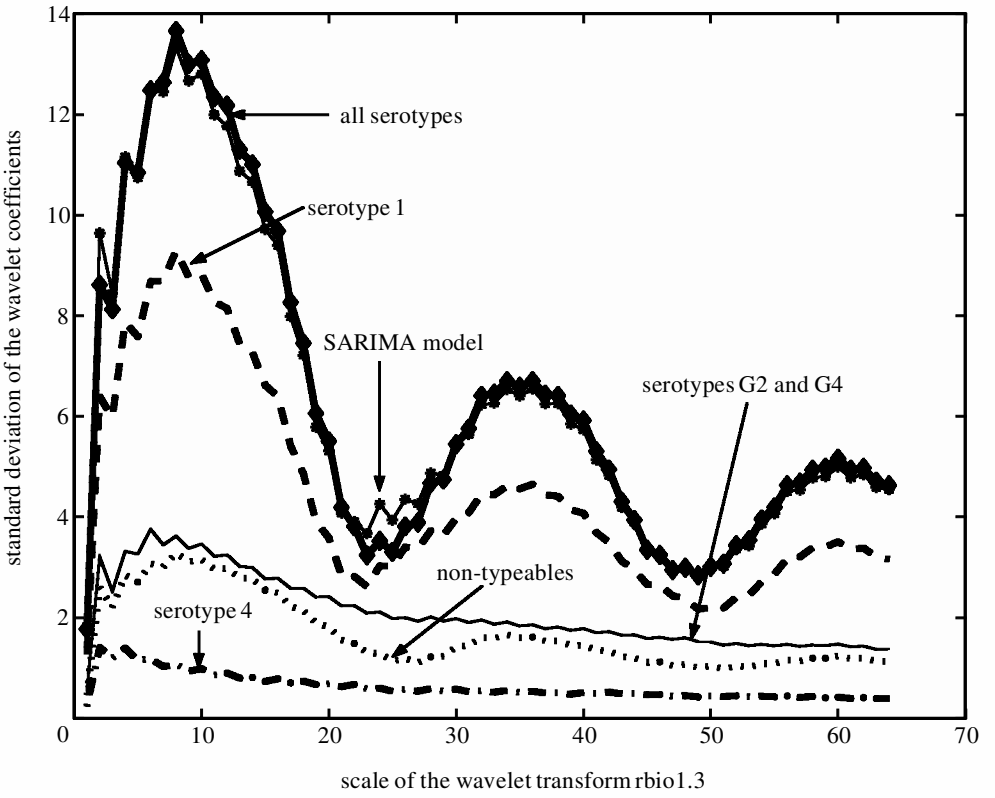


Figure 7. Wavelet coefficients standard deviation $\sigma_{wav}$ versus scale $a$ for the incidence of rotavirus using as an analysing wavelet rbio1.3. The arrows indicate the actual data; the SARIMA $(1, 0, 0) \times (3, 1, 0)_{12}$ model; serotypes G1, G2 and G3, G4, and non-typeables. The outcome is similar for other analysing wavelets.

ceeds not only because it eliminates trends in a mathematically acceptable way for a short time-series, but also because it crisply reveals ranges of scales over which the dynamics of incidence of rotavirus have different short- and long-term behaviour. The multifractal spectrum of the epidemics of rotavirus can be determined by means of WA (Muzy *et al.* 1994). It seems worthwhile to examine the hypothesis that this multifractal character of the rotavirus dynamics may provide a mechanism by which the epidemic may be more stable than by those mechanisms generated by classical scaling (West 1990).

From an epidemiological perspective, the detection of robust multiple scaling in the incidence of rotavirus is of interest because it indicates that the control mechanisms regulating the epidemic might interact as part of a coupled cascade of feedback loops in a system operating *far from equilibrium*. In this regard, the stability properties of the threshold of the epidemic as gauged by the so-called basic reproduction number (Ro) are to be determined. Modifications of the current mathematical model of rotavirus epidemic (e.g. José & Bobadilla 1994) considering the multifractal character of the dynamics are now underway.

Pastor-Satorras & Vespignani (2001*a*,*b*) have found that in scale-free networks there is not an epidemic threshold, which implies that infections can proliferate at whatever spreading rate the epidemic agent possesses. The reason behind the absence of a threshold for the spread of infection in the Pastor-Satorras & Vespignani (2001*a*,*b*) study is that their scale-free distribution has infinite variance and hence Ro always exceeds unity (Lloyd & May 2001). However, as shown in the calculation of the standard deviation of the wavelet coefficients as a function of the scale, it seems that the network of rotavirus epidemic does not seem to have infinite variance, although the rotavirus network is highly heterogeneous in size and durations of epidemic events.

This study has several strengths as well as potential limitations. The present study did not address the biological mechanisms underlying the observed changes in the dynamics of the incidence of rotavirus infections. We are dealing with rotavirus infections that produce severe acute gastroenteritis, requiring hospital admission for treatment, i.e. we have examined the dynamics of the disease rather than the dynamics of infections. We are just looking at a small piece of a larger picture.

The absence of a characteristic peak in a power-law degree distribution implies that in the rotavirus epidemic there is no such thing as a more virulent serotype. Therefore, immunological factors associated with the severity of the disease, other than viral properties, need to be sought. Studies of variations of immunity over time of the asymptomatic carriers are urgently needed to fully understand the biological mechanisms of the dynamics of rotavirus infection.

The application of any vaccine against rotavirus infection should consider the self-similarity (multifractality) and the self-coupling of the annual cycle of the dynamics of a rotavirus epidemic. The results of the present article may provide insights for the application and the development of a more effective and safer vaccine after the withdrawal of the human-rhesus reassortant tetravalent rotavirus oral vaccine due to the attributable risk of intestinal intussusception after vaccination (Abramson *et al.* 1999). In particular, we need to stop considering the

rotavirus serotypes separately. Rather, they constitute a community that acts in unison.

Despite all caveats which arise in describing a complex human biological phenomenon at the population level, the present mathematical analysis sheds some light upon the inherent dynamics of the epidemic of rotavirus.

M.V.J. was financially supported by PAPIIT-IN213199, UNAM, México. R.F.B. was supported by grants from the NHMRC and RCHRF. We thank Paul Masendycz, Sandra Dwyer, Lorraine Adams, Helen Bugg and Nada Bogdanovic-Sachran for being responsible of diagnosis and typing the rotavirus strains from 1977–2000. We also thank Claudia Lerma, Imelda López-Villaseñor, Tzipe Govezenski, Miguel A. Torres-Vega and Luis Padilla-Noriega for helpful comments on the manuscript and J. R. Bobadilla for help with data processing in the SARIMA models.

## APPENDIX A

### (a) *SARIMA models*

The SARIMA model is expressed as

$$\phi_p(B)\Phi_P(B^r)\mathcal{Y}_t = \theta_q(B)\Theta_Q(B^r)Z_t, \tag{A 1}$$

where $B$ denotes the backward shift operator, $\phi_p$, $\Phi_P$, $\theta_q$, $\Theta_Q$ are polynomials of order $p$, $P$, $q$ and $Q$ respectively, $Z_t$ denotes a purely random process, and

$$\mathcal{Y}_t = \nabla^d \nabla_r^D Y_t, \tag{A 2}$$

where $\nabla$ is the backward difference operator. The variables $\{\mathcal{Y}_t\}$ are formed from the original series $\{Y_t\}$ not only by simple differencing (to remove trend) but also by seasonal differencing, $\nabla_r$, to remove seasonality. For example, if $d = D = 1$, and $r = 1$, then

$$\mathcal{Y}_t = \nabla\nabla_{12} Y_t = \nabla_{12} Y_t - \nabla_{12} Y_{t-1},$$
$$\mathcal{Y}_t = (Y_t - Y_{t-12}) - (Y_{t-1} - Y_{t-13}).$$

The model in equations (A 1) and (A 2) is said to be a SARIMA model of order $(p, d, q) \times (P, D, Q)_r$.

### (b) *Definition of the periodogram*

The periodogram estimate of the PSD of a time-series of length $N$, $y_N(t)$ is

$$\hat{P}_{yy}(f) = \frac{|Y_N(f)|^2}{f_s N}, \tag{A 3}$$

where

$$Y_N(f) = \sum_{t=0}^{N-1} y_N(t) e^{-2\pi i f_t / f_s},$$

and $f_s$ is the sampling frequency.

### (c) *Definition of cumulants and the bispectrum*

Let us make the convenient assumption that the process has a zero mean. The second-order cumulant, denoted by $C2(i)$, is the autocovariance function. For a zero-mean process, $C2(i)$ and the third-order cumulant $C3(i, j)$, are identical with the second- $M2(i)$ and the third-order moment $M3(i, j)$, of the process, respectively, i.e.

$$\left.\begin{aligned} C2(i) &= M2(i) = E\{y(n)y(n+i)\} \\ C3(i, j) &= M3(i, j) = E\{y(n)y(n+j)y(n+i)\} \end{aligned}\right\}, \tag{A 4}$$

where the operator $E$ denotes the statistical expectation. If $y(n)$ is a Gaussian process, then its statistics are completely characterized by its autocorrelation function. If $y(n)$ is non-Gaussian, as are most real world signals, then it is not completely characterized by its autocorrelation function. The higher-order moments of the process carry information which is not contained in the autocorrelation function. Then, the cumulants of a Gaussian process are identically zero for orders greater than two, for example,

$$C3(i, j) = 0,$$
$$C4(i, j, k) = 0 \text{ etc.}$$

The bispectrum is a function of two frequencies and is defined by

$$S_{3y}(f_1, f_2) = \sum_{k=-\infty}^{\infty} \sum_{l=-\infty}^{\infty} C_{3y}(k, l) e^{-i2\pi f_1 k} e^{-i2\pi f_2 l}. \tag{A 5}$$

For a real-valued process, symmetry properties of cumulants carry over to symmetry properties of bispectra. The symmetry properties of the bispectrum can be found in Rao & Gabr 1984.

### (d) *Nonlinear processes: Volterra model*

The simplest nonlinear system is the second-order Volterra system whose input–output relationship is defined by

$$y(n) = \sum_{k=0}^{\infty} h(k)x(n-k) + \sum_{k=0}^{\infty} \sum_{l=0}^{\infty} q(k, l)x(n-k)x(n-l). \tag{A 6}$$

The corresponding frequency domain representation is

$$Y(f) = H(f)X(f) + \sum_{f_1+f_2=f_3} Q(f_1, f_2)X(f_1)X(f_2), \tag{A 7}$$

and is obtained by Fourier transforming both sides of (A 6). The time-domain product term $x(n-k)x(n-l)$ leads to convolution in the frequency domain, which is represented by the condition $f_3 = f_1 + f_2$. It is usually assumed that the quadratic kernel is real and symmetric, that is, $q(k, l) = q(l, k)$, or equivalently, $Q(f_1, f_2) = Q(f_2, f_1) = Q^*(-f_1, -f_2)$. It is readily verified that $Q(f_1, f_2)$ in the region $|f_2| \leqslant f_1$, $0 \leqslant f_1 \leqslant 1/4$, specifies $Q(f_1, f_2)$ everywhere.

We want to estimate the linear part, $h(k)$, and the quadratic part, $q(k, l)$ given $x(n)$ and, $y(n)$, $n = 1, \ldots, N$. In particular, the quadratic kernel in the second-order Volterra model is usually assumed to be symmetric. A least-squares formulation to estimate the linear and the quadratic part of the Volterra model will involve second-, third- and fourth-order moments. The QPC problem is a special case where the linear part is zero, the quadratic part is diagonal and $x(n)$ is a sum of harmonics (see equation (A 6)).

It is important to note that consistent estimates of the bispectrum ($C_{3y}(\tau_1, \tau_2)$) will be obtained from a single realization, only if frequency coupling is always accompanied by phase coupling (Swami & Mendel 1990). Given a single realization, $C_{3y}(\tau_1, \tau_2)$ will show impulses if frequency coupling exists, that is, $f_3 = f_2 + f_1$. Given multiple realizations, $C_{3y}(\tau_1, \tau_2)$ (and $C_{3y}(\tau, \tau)$) will be non-zero only if both frequency and phase coupling exist, that is, $f_3 = f_2 + f_1$, and $\phi_3 = \phi_2 + \phi_1$ (Swami *et al.* 1998).

### (e) *Detrending fluctuation analysis*

The DFA method comprises the following steps (Peng *et al.* 1993, 1994): the incidence interval time-series (of total length $N$) is first integrated, $y(k) = \Sigma_{i=1}^{k}[B(i) - B_{\mathrm{ave}}]$, where $B(i)$ is the $i$th incidence interval and $B_{\mathrm{ave}}$ is the average incidence interval. Next the integrated time-series is divided into boxes of equal length, $n$. In each box of length $n$, a least-squares line is fitted to the data (representing the trend in that box). The $y$ coordinate of the straight line segments is denoted by $y_n(k)$. Next, the integrated time-series, $y(k)$, is detrended by subtracting the local trend, $y_n(k)$, in each box. The root mean square fluctuation of this integrated and detrended time-series is calculated by

$$F(n) = \sqrt{\frac{1}{N}\sum_{k=1}^{N}[y(k) - y_n(k)]^2}. \qquad \text{(A 8)}$$

This computation is repeated over all time-scales (box sizes) to provide a relationship between $F(n)$, the average fluctuation as function of box size, and the box size $n$ (i.e. the number of cases in a box which is the size of the window of observation).

### (f) *Definition of the WT*

We introduce the one-dimensional continuous WT and some of the basic mathematical results. We consider a function $s(t)$ in the Hilbert space $L^2(\boldsymbol{R}, \mathrm{d}t)$. We decompose this function $s$ in terms of elementary functions obtained by dilations and translations of the real valued mother function $\Psi(t)$. Let us define $\Psi_{a,b} = a^{-1/2}\Psi((t-b)/a)$. The WT of $s(t)$ is defined as (Daubechies 1994)

$$T_{\Psi}[s](a,b) = \langle \Psi_{a,b} | s \rangle_{L^2(\mathbf{R},\mathrm{d}t)} = a^{-1/2}\int_{-\infty}^{\infty}\Psi\left(\frac{t-b}{a}\right)s(t)\mathrm{d}t, \qquad \text{(A 9)}$$

where $\langle \cdot | \cdot \rangle_{L^2(\mathbf{R},\mathrm{d}t)}$ is the scalar product in $L^2(\boldsymbol{R}, \mathrm{d}t)$. Thus the WT is basically the scalar product of the function with the analysing wavelet dilated by $a$ and translated by $b$.

## REFERENCES


Abramson, J. S. (and 11 others) 1999 Possible association of intussusception with rotavirus vaccination. *Pediatrics* **104**, 575.

Akaike, H. A. 1979 Bayesian extension of the minimum AIC procedure of autoregressive fitting. *Biometrika* **66**, 237–242.

Ansari, S. A., Springthorpe, V. S. & Sattar, S. A. 1991 Survival and vehicular spread of human rotaviruses: possible relation to seasonality of outbreaks. *Rev. Inf. Dis.* **13**, 448–461.

Barnes, G. L., Uren, E., Stevens, K. B. & Bishop, R. F. 1998 Etiology of acute gastroenteritis in hospitalised children in Melbourne, Australia from April 1980 to March 1993. *J. Clin. Microbiol.* **36**, 133–138.

Bern, C., Unicomb, L., Gentsch, J. L., Banul, L., Yunus, M., Sack, B. & Glass, R. I. 1992 Rotavirus diarrhoea in Bangladeshi children: correlation of disease severity with serotypes. *J. Clin. Microbiol.* **30**, 3234–3238.

Bishop, R. F. 1986 Epidemiology of diarrhoeal disease caused by rotavirus. In *Development of vaccines and drugs against diarrhea* (ed. J. Holmgren & A. Lundberg), pp. 158–170. Lund, Sweden: Student literature.

Bishop, R. F. 1994 Natural history of human rotavirus infection. In *Viral infections of the gastrointestinal tract*, 2nd edn (ed. A. Z. Kapikian), pp. 131–167. New York: Dekker.

Bishop, R. F., Unicomb, L. E. & Barnes, G. L. 1991 Epidemiology of rotavirus serotypes in Melbourne, Australia, from 1973 to 1989. *J. Clin. Microbiol.* **29**, 862–888.

Box, G. E. P. & Jenkins, J. M. 1976 *Time series analysis: forecasting and control*. San Francisco, CA: Holden-Day.

Brandt, C. D. (and 10 others) 1983 Pediatric viral gastroenteritis during eight years of study. *J. Clin. Microbiol.* **18**, 71–78.

Cascio, C., Vizzi, E., Alaimo, C. & Arista, S. 2001 Rotavirus gastroenteritis in Italian children: can severity be related to the infecting virus? *Clin. Inf. Dis.* **32**, 1126–1132.

Daubechies, I. 1994 Ten lectures on wavelets. *CBMS, SIAM* **61**, 271–280.

De Zoyza, I. & Feachem, R. G. 1985 Interventions for the control of diarrhoeal diseases among young children: rotavirus and cholera immunization. *Bull. WHO* **63**, 569–583.

Estes, M. K. & Cohen, J. 1989 Rotavirus gene structure and function. *Microbiol. Rev.* **53**, 410–449.

Grenfell, B. T., Bjørnstad, O. N. & Kappey, J. 2001 Travelling waves and spatial heterogeneities in measles epidemics. *Nature* **414**, 716–723.

Heneghan, C. & McDarby, G. 2000 Establishing the relation between detrended fluctuation analysis and power spectral density analysis for stochastic processes. *Phys. Rev.* E **62**, 6103–6110.

José, M. V. & Bobadilla, J. R. 1994 Epidemiological model of diarrhoeal diseases and its application in prevention and control. *Vaccine* **12**, 109–116.

José, M. V., Bobadilla, J. R. & Bishop, R. F. 1996 Oscillatory fluctuations in the incidence of rotavirus infections by serotypes 1, 2, 3, and 4. *J. Diarrhoeal Dis.* **14**, 194–200.

Kapikian, A. Z. & Chanock, R. M. 1996 Rotaviruses. In *Fields virology* (ed. B. N. Fields, D. N. Knipe & P. M. Howley), pp. 1657–1708. New York: Raven Press.

LeBaron, C. W., Lew, J., Glass, R. I., Weber, J. M. & Ruiz, G. M. 1990 Annual rotavirus epidemic patterns in North America: results of a 5-year retrospective survey of 88 centers in Canada, Mexico, and the United States. *JAMA* **264**, 983–988.

Liljeros, F., Edling, C. R., Amaral, L. A. N., Stanley, H. & Aberg, Y. 2001 The web of human sexual contacts. *Nature* **411**, 907–908.

Lloyd, A. L. & May, R. 2001 M. 2001 How viruses spread among computers and people. *Science* **292**, 1316–1317.

Masendycz, P. J., Unicomb, L. E., Kirkwood, C. D. & Bishop, R. F. 1994 Rotavirus serotypes causing severe acute diarrhoea in young children in six Australian cities, 1988 to 1992. *J. Clin. Microbiol* **32**, 2315–2317.

Masendycz, P. J., Bogdanovic-Sakran, N., Kirkwood, C. D., Bishop, R. F. & Barnes, G. 2001 Report of the Australian rotavirus surveillance program, 2000/2001. *Commun. Dis. Intell.* **25**, 143–146.

Misiti, M., Misiti, Y., Oppenheim, G. & Poggi, J.-M. 2000 *Wavelet toolbox, Matlab user's guide v. 2*, R12. Natick, MA: The Math Works Inc.

Montroll, E. W. & Shlesinger, M. F. 1984 On the wonderful world of random walks. In *Nonequilibrium phenomena II: from stochastic to hydrodynamics* (ed. E. W. Montroll), pp. 288–293. Amsterdam: North Holland.

Muzy, J. F., Bacry, E. & Arneodo, A. 1994 The multifractal formalism revisited with wavelets. *Int. J. Bifurcation Chaos* **4**, 245–302.

Padilla-Noriega, L., Arias, C. F., Lopez, S., Puerto, F., Snodgrass, D. R., Taniguchi, K. & Greenberg, H. B. 1990 Diversity of rotavirus serotypes in Mexican infants with gastroenteritis. *J. Clin. Microbiol.* **28**, 1114–1119.

Pastor-Satorras, R. & Vespignani, A. 2001*a* Epidemic spreading in scale-free networks. *Phys. Rev. Lett.* **86**, 3200–3203.

Pastor-Satorras, R. & Vespignani, A. 2001*b* Epidemic dynam-

ics and endemic states in complex networks. *Phys. Rev.* E **63**, 066117.

Peng, C.-K., Buldyrev, S. V., Goldberger, A. L., Havlin, S., Simons, M. & Stanley, H. E. 1993 Finite-size effects on long-range correlations: implications for analysing DNA sequences. *Phys. Rev.* E **47**, 3730–3733.

Peng, C.-K., Buldyrev, S. V., Havlin, S., Simons, M., Stanley, H. E. & Goldberger, A. L. 1994 Mosaic organization of DNA nucleotides. *Phys. Rev. Lett.* **49**, 1685–1689.

Peng, C.-K., Havlin, S., Stanley, H. E. & Goldberger, A. R. 1995 Quantification of scaling exponents and crossover phenomena in non-stationary heartbeat time series. *Chaos* **5**, 82–87.

Priestley, M. B. 1988 *Nonlinear and non-stationary time series analysis*. London: Academic.

Rao, S. & Gabr, M. 1984 *An introduction to bispectral analysis and bilinear time-series models*. New York: Springer.

Rhodes, C. J. & Anderson, R. M. 1996 Power laws governing epidemics in isolated populations. *Nature* **381**, 600–602.

Schwarz, G. 1978 Estimating the dimension of a model. *Ann. Stat.* **6**, 461–464.

Shlesinger, M. F. 1987 Fractal time and 1/*f* noise in complex systems. *Ann. NY Acad. Sci.* **504**, 214–228.

Shumway, R. H. 1988 *Applied statistical time-series analysis*. Englewood Cliffs, NJ: Prentice-Hall.

Sprott, J. C. & Rowlands, G. 1995 *Chaos data analyzer. The professional version*. New York: American Institute of Physics.

Stratonovich, R. L. 1963 *Topics in the theory of random noise*, vol. I. New York: Gordon and Breach.

Swami, A. & Mendel, J. M. 1990 ARMA parameter estimation using only output cumulants. *IEEE Trans. ASSP* **38**, 1257–1265.

Swami, A., Mendel, J. M. & Nikias, C. L. 1998 *Higher-order spectral analysis toolbox. For use with* MATLAB. Natick, MA: The Math Works.

Theiler, J., Eubank, S., Longtin, A., Galdrikian, B. & Farmer, J. D. 1992 Testing for nonlinearity in time series: the method of surrogate data. *Physica* D **58**, 77–94.

Tick, L. J. 1961 The estimation of 'transfer functions' of quadratic systems. *Technometrics* **3**, 563–567.

Velazquez, F. R., Calva, J. J., Guerrero, M. L., Mass, D., Glass, R. I., Pickering, L. K. & Ruiz-Palacios, M. 1993 Cohort study of rotavirus serotype patterns in symptomatic and asymptomatic infections in Mexican children. *Pediatr. Infect. Dis.* **2**, 54–61.

West, B. C. 1990 Fractal forms in physiology. *Int. J. Mod. Phys.* **4**, 1629–1669.

West, B. C. & Shlesinger, M. F. 1989 On the ubiquity of 1/*f* noise. *Int. J. Mod. Phys.* B **6**, 795–819.

Woods, P. A., Gentsch, J., Gouvea, V., Mata, L., Simhon, A., Santosham, M., Bai, Z. S., Urasawa, S. & Glass, R. 1992 Distribution of serotypes of human rotavirus in different populations. *J. Clin. Microbiol.* **30**, 781–785.

Zhou, G. & Giannakis, G. B. 1994 Self coupled harmonics: stationary and cyclostationary approaches. In *Proc. Int. Conf. on Acoustics, Speech and Signal Processing, Adelaide, Australia, 19–22 April 1994*, XII Congress of IUSSI, pp. 153–156.